Published in final edited form as:
Cell. 2014 July 31; 158(3): 647–658. doi:10.1016/j.cell.2014.05.043.

Stochastic but highly coordinated protein unfolding and translocation by the ClpXP proteolytic machine

Juan Carlos Cordova[1,†], **Adrian O. Olivares**[2,†], **Yongdae Shin**[3,†], **Benjamin M. Stinson**[2], **Stephane Calmat**[2,4], **Karl R. Schmitz**[2], **Marie-Eve Aubin-Tam**[5], **Tania A. Baker**[2,4], **Matthew J. Lang**[1,6,*], and **Robert T. Sauer**[2,*]

[1]Department of Chemical and Biomolecular Engineering, Vanderbilt University, Nashville, TN 37235. [2]Department of Biology, Massachusetts Institute of Technology, Cambridge, MA 02139. [3]Department of Mechanical Engineering, Massachusetts Institute of Technology, Cambridge, MA 02139. [4]Howard Hughes Medical Institute, Massachusetts Institute of Technology, Cambridge, MA 02139. [5]Department of Bionanoscience, Kavli Institute of Nanoscience, Delft University of Technology, Lorentzweg 1, 2628 CJ Delft, The Netherlands. [6]Department of Molecular Physiology and Biophysics, Vanderbilt University School of Medicine, Nashville, TN 37235.

Abstract

CIpXP and other AAA+ proteases recognize, mechanically unfold, and translocate target proteins into a chamber for proteolysis. It is not known if these remarkable molecular machines operate by a stochastic or sequential mechanism or how power strokes relate to the ATP-hydrolysis cycle. Single-molecule optical trapping allows CIpXP unfolding to be directly visualized and reveals translocation steps of ~1–4 nm in length, but how these activities relate to solution degradation and the physical properties of substrate proteins remains unclear. By studying single-molecule degradation using different multi-domain substrates and CIpXP variants, we answer many of these questions and provide evidence for stochastic unfolding and translocation. We also present a mechanochemical model that accounts for single-molecule, biochemical, and structural results, for our observation of enzymatic memory in translocation stepping, for the kinetics of translocation steps of different sizes, and for probabilistic but highly coordinated subunit activity within the CIpX ring.

*corresponding authors (matt.lang@vanderbilt.edu; bobsauer@mit.edu).
†These authors contributed equally to this work.

Author contributions. J.C.C., A.O.O., and Y.S. performed and/or analyzed optical-trapping experiments. B.M.S. performed the Fig. 6 experiments. S.C., K.R.S., and A.O.O. constructed and purified substrates and enzymes for single-molecule experiments. A.O.O., M.A-T., and M.J.L. built the optical traps. R.T.S. developed the Fig. 7 models. All authors contributed to writing the manuscript.

Introduction

AAA+ proteases (ATPases associated with diverse cellular activities) maintain protein quality control in the cell by converting the energy derived from ATP binding and hydrolysis into work that powers mechanical protein unfolding, translocation, and ultimately degradation (Sauer and Baker, 2011). How these destructive enzymes degrade proteins with widely varying sequences, structures, and stabilities is only beginning to be understood. ClpXP, one of the best-characterized members of this family of degradation machines, consists of ClpX, a hexameric AAA+ ATPase, and ClpP, a barrel-shaped peptidase (Baker and Sauer, 2012). Degradation is initiated when the ClpX ring binds a substrate via an unstructured degron, such as the ssrA tag, and attempts to translocate this peptide through its narrow axial pore. For native substrates, degron translocation by ClpX pulls on the folded portion of the protein, driving mechanical denaturation that allows subsequent translocation steps to spool the unfolded polypeptide into ClpP for degradation.

Single-molecule studies, using optical tweezers to monitor ClpXP unfolding and translocation of multi-domain substrates, establish that ClpXP can work against forces of 20 pN or higher, demonstrate that the smallest translocation steps are ~1 nm (~4–8 amino acids), and reveal physical steps that are multiples of this value, resulting from kinetic bursts of two, three, or four power strokes (Aubin-Tam et al. 2011; Maillard et al., 2011; Sen et al., 2013). Studies of variants containing inactive subunits support a probabilistic mechanism of ATP hydrolysis and mechanical function by ClpXP (Martin et al., 2005), but this model is not firmly established, and a related AAA+ protease has been proposed to operate by a sequential mechanism (Smith et al., 2011). At present, it is not known how the physical properties of native and unfolded substrates affect the kinetics of single-molecule ClpXP unfolding and translocation or if these reactions account for solution-degradation rates. Moreover, no current model satisfactorily explains how the ClpX ring generates translocation steps of different sizes, accounts for the kinetics of unfolding and translocation, or explains the linkage between ATP consumption and these mechanical reactions. Any deep understanding of AAA+ proteases and related remodeling machines requires answers to these questions.

Here, we use optical trapping to assay single-molecule ClpXP unfolding and translocation of substrates consisting of domains with varying stabilities and sequences. We find that ClpXP unfolds most domains by a single pathway, with kinetics that depend on the native fold and structural stability. Subsequent translocation or pausing occurs at rates that vary with the sequence of the unfolded substrate. During translocation, ClpXP does not exhibit a sequential pattern of step sizes, supporting a fundamentally stochastic reaction, but a mechanism of enzymatic memory results in short physical steps being more probable after short steps and longer physical steps being more likely after longer steps, allowing the enzyme to run at different speeds. Surprisingly, two ATP-hydrolysis events can drive more than two power strokes, as an engineered ClpX hexamer with just two active subunits also takes ~1–4 nm physical steps. Finally, we show that solution proteolysis is many times slower than predicted from single-molecule results. We discuss the implications of these results for understanding ClpXP structure and biological function and present a mechanochemical model in which initial stochastic ATP hydrolysis in the AAA+ ring can be

followed by a cascade of coordinated power strokes. This model explains our single-molecule results and also accounts for a wide range of previous biochemical, genetic, and structural results.

Results

Substrate design and single-molecule degradation

CIpXP degrades ssrA-tagged variants of the titin^{127} domain at different rates (Kenniston et al., 2003). For example, the V13P and V15P mutations disrupt or eliminate hydrogen bonds close in space to the C-terminal ssrA tag (Figs. 1A, 1B), reduce thermodynamic, kinetic, and mechanical stability, and accelerate CIpXP degradation, with the wild-type (WT) domain being most stable and degradation resistant, V15P having intermediate stability and degradation rates, and V13P being least stable and most rapidly degraded (Li et al., 2000; Kenniston et al., 2003). For single-molecule studies, we constructed Halo-WT-WT-WT-WT-ssrA, Halo-V13P-V13P-V13P-V13P-ssrA, Halo-V15P-V15P-V15P-V15P-ssrA, and Halo-WT-V13P-V13P-V13P-ssrA substrates, in which Halo is an N-terminal HaloTag domain that allows covalent attachment to a biotinylated DNA spacer. For optical-trapping (Fig. 1C), multi-domain substrates were attached via the Halo domain and DNA spacer to one streptavidin-coated bead, and a biotinylated variant of CIpXP was attached to a second streptavidin-coated bead (Aubin-Tam et al., 2011). In all substrates, the Halo domain was connected to the adjacent titin domain by a 22-residue linker, whereas the remaining titin domains were connected by 4-residue linkers.

Optical-trapping measurements under constant force (Aubin-Tam et al., 2011) were used to visualize single-molecule CIpXP unfolding and translocation. Individual traces displayed three signatures of CIpXP mechanical function as shown in Fig. 1D. First, abrupt increases in bead-to-bead distance occurred upon unfolding, with the size of the transition being smaller for titin domains than for the Halo domain. Second, bead-to-bead distance decreased following unfolding, as CIpXP translocated the unfolded polypeptide, with the total decrease depending upon the size of the denatured domain and the length of the linker to the next domain. Third, between completed translocation of one unfolded domain and denaturation of the next native domain, there was a pre-unfolding dwell with little change in bead-to-bead distance.

Pre-unfolding dwell times depend on substrate stability

The pre-unfolding dwell represents the time that CIpXP pulls on a native protein domain before denaturation occurs. Pre-unfolding dwells for the first unfolding event in each trajectory were not quantified, as recording began after some attempted unfolding, unfolding, or translocation by CIpXP had occurred. For example, the second and fourth traces in Fig. 1D contain just three titin unfolding events and one Halo unfolding event. Because there are four titin domains in the multi-domain substrate, one V15P or V13P domain must have been unfolded and translocated before these traces began.

CIpXP unfolding of a protein domain typically requires many ATP-hydrolysis events (Kenniston et al., 2003). If enzymatic unfolding occurs by a single pathway and one rate-

limiting kinetic step, then pre-unfolding dwells should be exponentially distributed. Multiple unfolding pathways with one rate-limiting step would give dwells distributed as a sum of exponentials, whereas multiple kinetic steps with similar time constants would give a gamma distribution of dwell times. For CIpXP unfolding of V13P (N = 278 events), V15P (N = 127 events), and Halo (N = 73 events), the pre-unfolding dwell distributions fit well to single exponentials ($R^2 \geq 0.987$), with average unfolding times (τ_{unf}) of 5.9, 17, and 8.7 s, respectively (Figs. 2A–2C). Only 17 WT unfolding events, some of which may be CIpXP independent (see Supplemental Results), were observed in ~200 experiments, indicating that most experiments terminated before WT unfolding. Indeed, some Halo-WT-V13P-V13P-V13P-ssrA traces contained three V13P unfolding events, a long terminal dwell, and rupture of the bead-bead tether before CIpXP could unfold the WT domain (Fig. 2D). Including WT pre-unfolding dwells and these terminal dwells, which represent a lower bound of the pre-unfolding dwell, gave an exponential distribution with τ_{unf} ~55 s (N = 41; Fig. 2E). Fitting just the WT pre-unfolding dwells gave a τ_{unf} about half this value, which was unrealistically small given the distribution of terminal dwells. Rates of CIpXP unfolding in the order V13P > V15P > WT are consistent with the relative stabilities of these domains (Li et al., 2000; Kenniston et al., 2003). Thus, destabilizing mutations proximal to the site of CIpXP pulling result in faster enzymatic denaturation. The exponential distribution of pre-unfolding dwells for these proteins indicates that one kinetic step is largely rate limiting for CIpXP unfolding, a finding supported by inspection of the randomness of the process (see Supplemental Results). Models with parallel faster and slower exponential processes improved the residuals of the V13P and V15P fits modestly (Fig. S1), consistent with the possibility of two unfolding pathways (see Discussion).

Force has opposing effects, reducing CIpXP activity but also destabilizing domains in the substrate to a degree that depends on the distance to the unfolding transition state (Carrion-Vazquez et al., 1999). We ranked pre-unfolding dwells by force, calculated averages over a moving window, and plotted average dwell time against average force (Figs. 2F & 2G). Unfolding of V13P and V15P was faster at higher force (Fig. 2F), suggesting that force destabilizes these titin domains more than it decreases CIpXP activity. By contrast, Halo unfolding was slower at higher force, suggesting that force destabilizes Halo less than it decreases CIpXP activity, a result consistent with the distance to the transition state being smaller for CIpXP unfolding of Halo than the titin domains (Li et al., 2000; Popa et al., 2013). The ratios of CIpXP-dependent to CIpXP-independent unfolding events were ~20, ~7 and ~1 for the V13P, V15P and WT domains, respectively, a trend consistent with distances to the unfolding transition state determined from atomic-force microscopy experiments for these domains (Li et al., 2000; see Supplemental Results).

Translocation velocity and pausing

CIpXP translocation typically proceeded monotonically, but pauses longer than 2.5 s were occasionally observed (Fig. 3A). After subtracting these pauses, we calculated average translocation velocities. The V13P, V15P, and WT velocities were similar, as expected because these sequences differ at only one residue position. For 656 pooled titin translocation traces, the mean velocity was 24 ± 0.4 aa s^{-1} (4.4 ± 0.1 nm s^{-1}), where the errors are SEM values. For 78 Halo translocation traces, the mean velocity was slower (18 ±

0.8 aa s^{-1}; 3.3 ± 0.1 nm s^{-1}). Thus, the polypeptide sequence has a modest impact on CIpXP translocation velocity, a result consistent with biochemical studies (Barkow et al., 2009). Fig. 3B shows average translocation velocities plotted against average force. Fitting these data gave unloaded translocation velocities of 29 aa s^{-1} for titin domains and 20 aa s^{-1} for Halo domains.

Pausing occurred with higher probability at some titin and Halo sequences (Fig. 3C, 3D) and was less common during translocation of titin (3.7% of events) than Halo (17% of events). Sequence dependent pausing could occur either because of direct interactions of the translocating polypeptide with CIpXP or because some sequences have a higher probability of forming transient structure that impedes translocation.

Stochastic steps of different size and kinetic complexity contribute to translocation

Using a chi-squared algorithm (Kerssemakers et al., 2006), we resolved individual physical steps in a subset of translocation traces with good signal to noise (for examples, see Fig. 4A). As reported (Aubin-Tam et al., 2011; Maillard et al., 2011; Sen et al., 2013), the smallest physical steps were ~1 nm but many steps were 2-fold, 3-fold, and 4-fold larger (Figs. 4A, 4B). Force had little effect on the average step length (~2 nm; Fig. 4C), and complete translocation of each titin domain (~90 residues) required an average of ~8 physical steps (Fig. 4D).

During titin translocation, the dwell times both preceding and following a physical step increased with the size of the step (Fig. 4E). The dwell times for pooled steps of all sizes (Fig. 4F) and for individual steps of different sizes (Fig. S2) were distributed non-exponentially, suggesting that multiple kinetic steps contribute to each physical translocation step. Importantly, there was no strong sequential pattern of step sizes (Fig. 4G). In the trajectories shown in Fig. 4A, for example, the order of steps was 1-2-1-1-1-2-3-3-1-1 for the leftmost trace, 3-2-2-2-3-4 for the center trace, and 1-1-1-1-1-2-2-3-2-2-1-1 for the rightmost trace. Despite the absence of a clear pattern, 1 nm steps had a higher probability of being preceded or followed by another 1 nm step compared to longer steps, and steps of 2–4 nm also tended to be preceded and followed by longer steps (Fig. 4G). These results support a stochastic mechanism of subunit firing with some degree of motor memory. CIpXP translocation of the Halo domain also showed a distribution of steps ranging from ~1–4 nm (Fig. S3).

To investigate mechanism independently of the detection of individual steps, we calculated times from the beginning to the end of translocation of V13P and V15P domains followed by the 4-residue linker (93 total residues; N = 387) and subtracted any pauses. The histogram of completion times showed multiple peaks (Fig. 4H), supporting populations of faster and slower moving enzymes, a finding consistent with our observation that CIpXP has an increased probability of taking short steps after short steps and *vice versa*.

Unfolding, translocation, and pausing by a hobbled CIpX motor

To determine the effects of eliminating ATP hydrolysis in multiple CIpX subunits, we used a variant containing two subunits with ATPase-defective R370K sensor-II mutations (R),

two wild-type subunits (W), and two subunits with ATPase-defective E185Q Walker-B mutations (E) in the order RWERWE. The ATPase defective subunits in this CIpX variant, which supports degradation of ssrA-tagged V13P, V15P, and WT titin substrates at 15–30% of wild-type CIpXP rates, can still bind and release nucleotide (Joshi et al., 2004; Hersch et al., 2005; Martin et al., 2005). In optical-tweezer experiments, we observed RWERWE CIpXP unfolding and translocation of V13P domains in Halo-V13P-V13P-V13P-V13P-ssrA (Fig. 5A) at forces up to 10.4 pN, whereas the wild-type enzyme was active at forces as high as 26 pN. An exponential fit of pre-unfolding dwell times for RWERWE CIpXP gave a τ_{unf} of 50 s (N = 19; Fig. 5B), corresponding to ~8-fold slower unfolding than by CIpXP with six active subunits. In experiments using Halo-V15P-V15P-V15P-V15P-ssrA or Halo-WT-WT-WT-WT-ssrA, we detected no RWERWE CIpXP unfolding. Thus, preventing ATP hydrolysis in four CIpX subunits dramatically slows the rate of unfolding of V13P, the least stable of the three titin-domain variants tested, and makes enzymatic unfolding of the V15P and WT domains too slow to detect under the forces used for optical trapping.

For V13P translocation by RWERWE CIpXP, the average translocation velocity after removing pauses was 5.7 ± 0.5 aa s^{-1}, a rate ~4-fold slower than CIpXP. Pauses defined as dwells longer than 7.5 s were present in ~45% of RWERWE traces, whereas pauses defined as dwells longer than 2.5 s were present in fewer than 4% of wild-type CIpXP traces. Thus, a CIpX ring with just two active subunits pauses more frequently and for longer times than a ring with six active subunits. The dwells between RWERWE CIpXP translocation steps were substantially longer than between CIpXP translocation steps (Figs. 5C, 5D). Strikingly, however, individual physical steps in RWERWE CIpXP translocation traces also ranged from ~1–4 nm (Figs. 5C, 5D). We conclude that large physical steps do not require ATP hydrolysis in more than two CIpX subunits.

Commitment is a slow step in solution degradation

Previous studies show that CIpP proteolysis is not a slow step in degradation (Thompson and Maurizi, 1994; Kenniston et al., 2003). How well do average times of unfolding (τ_{unf}) and translocation (τ_{trans}) determined in single-molecule experiments predict average degradation times determined at substrate saturation ($\tau_{deg} = 1/V_{max}$) in solution? If the average commitment time (τ_c) is defined to satisfy the equation $\tau_c + \tau_{unf} + \tau_{trans} = \tau_{deg}$, then $\tau_{unf} + \tau_{trans} \approx \tau_{deg}$ only when τ_c is small compared to $\tau_{unf} + \tau_{trans}$. For six substrates of varying stability, a plot of ($\tau_{unf} + \tau_{trans}$) against τ_{deg} gave a linear correlation with a slope of ~0.25 (Fig. 6A), indicating that solution degradation is ~4-times slower than expected from single-molecule unfolding and translocation. Although differences in conditions between solution and single-molecule experiments could account for some variation (see Fig. 6A legend), this result suggests that τ_c is the slow step in solution degradation or that ~75% of CIpXP enzymes are inactive, as calculation of V_{max} assumes 100% activity. To distinguish between these possibilities, we monitored single-turnover binding and unfolding of GFP-ssrA by a 20-fold molar excess of CIpXP (5- to 20-fold excess over K_M) at a series of temperatures and fit the exponential trajectories to determine τ values (Fig. 6B). We also performed steady-state degradation at each temperature to determine τ_{deg} (Fig. 6C), K_M for protein substrate (Fig. 6D), and measured rates of ATP hydrolysis in the presence of saturating GFP-ssrA (Fig. 6E). To calculate fractional activity, we added the time expected

for GFP translocation to the single-turnover τ values for binding/unfolding and divided this time by τ_{deg}. The fractional ClpXP activity was ~0.4 at 15 °C and increased to ~0.9 at 37 °C (Fig. 6F). The latter result indicates that ClpXP is ~90% active, a result consistent with previous studies (Hersch et al., 2005; Shin et al., 2009). Lower "activity" at lower temperatures may be a consequence of more ClpXP enzymes assuming a conformation that does not support substrate binding or activity.

The time required for ClpXP unfolding of pre-engaged GFP in solution is ~6 s at 30 °C (Martin et al., 2008a). Subtracting this time from the 34 s required to bind and unfold GFP in our single-turnover experiment at 30 °C yields a τ_c of 28 s, which is ~4.5-fold longer than the pre-engaged unfolding time. As τ_{deg} is substantially longer than $\tau_{unf} + \tau_{trans}$ even for substrate proteins with marginal stability (Fig. 6A), τ_c represents much of the time required for ClpXP degradation and appears to increase in proportion to substrate stability. For ClpXP degradation of wild-type titin^{127} substrates, cycles of binding, attempted engagement and/or unfolding, and substrate release contribute to the time needed for degradation (Kenniston et al., 2005). The linearity of the Fig. 6A plot suggests that similar cycles of substrate binding and release contribute to the degradation time required for many substrates.

Discussion

Domain stability and ClpXP unfolding

Matouschek and colleagues first reported that the local stability of structural elements adjacent to the degradation tag determined resistance to enzymatic unfolding (Lee et al., 2001). Our results support their model, as we find that mutations that decrease stability by altering hydrogen bonds to the C-terminal β-strand of titin also decrease the average pre-unfolding dwell time in single-molecule ClpXP experiments. However, rates of ClpXP degradation are not always correlated with global stability. For example, ClpXP degrades an ssrA-tagged variant of a hyperstable RNase-H (ΔG_u = 12 kcal/mol) faster than it degrades V13P-titin^{127}-ssrA ($\Delta G_u \approx$ 3 kcal/mol) (Kenniston et al., 2003; 2004). In RNase-H-ssrA, ClpXP initially pulls against a C-terminal helix as opposed to pulling against a β-strand in titin. Lee et al. (2001) speculated that AAA+ proteases might be able to unfold an α-helix, which can be pulled apart by stepwise unzipping, more easily than a strand in a β-sheet, which requires simultaneous shearing of multiple hydrogen bonds (Fig. S4). In the absence of force, our results suggest that ClpXP unfolds the Halo domain, which has a C-terminal helix, substantially faster than any of the titin domains, supporting the possibility that helices are inherently easier to unfold than strands in β sheets.

To a first approximation, the pre-unfolding dwell times for the V13P, V15P, and Halo domains were exponentially distributed, supporting one major unfolding pathway and a single rate-limiting kinetic step. Nevertheless, unfolding times were substantially longer than times required for even a burst of power strokes (~0.6 s based on the ATPase rate and translocation dwells), as expected if unfolding requires coincidence between a power stroke and transient stochastic thermal destabilization. Because most protein domains fold cooperatively, ClpXP disruption of even a small number of stabilizing native interactions could result in rapid global unfolding of the remaining structural elements in the domain. At

a second level, CIpXP unfolding of V13P fit better to exponential processes acting on less-stable and more-stable populations of similar size (Fig. S1), with enough events (N = 262) to make sampling error unlikely. This result is consistent with the existence of two unfolding pathways, which could depend upon which parts of the V13P domain are stochastically destabilized. For example, the N-terminal portion of V13P might be transiently frayed in the more-stable population and the C-terminal region transiently frayed in the less-stable population.

A model for unfolding, different physical step sizes, and motor memory

We find that a substantial number of physical translocation steps occur in multiples of ~1 nm, in agreement with previous results (Aubin-Tam et al., 2011; Maillard et al., 2011; Sen et al., 2013). Based on structures of CIpX rings, conformational changes larger than 1 nm seem unlikely, and it is commonly assumed that a ~1 nm step involves hydrolysis of one ATP and one power-stroke (Glynn et al., 2009; Aubin-Tam et al., 2011; Maillard et al., 2011; Sen et al., 2013; Stinson et al., 2013). Thus, bursts involving multiple power strokes are likely to drive larger physical steps. For wild-type CIpXP, each power stroke could result either directly or indirectly from hydrolysis of one ATP, as a CIpX hexamer binds a maximum of four ATPs (Hersch et al., 2005). Despite having just two catalytically active subunits, however, RWERWE CIpXP also takes physical steps ranging from ~1–4 nm, raising the possibility that a single ATP-hydrolysis event can generate more than one power stroke. For example, an initial power stroke might be generated by ATP hydrolysis and ADP/P_i release in one subunit and a subsequent power stroke by ATP dissociation from an inactive subunit in RWERWE CIpX (see below).

Any model of CIpXP function needs to be consistent with structural and biochemical results. For example, subunits in the CIpX hexamer display structural and biochemical asymmetry, suggesting a large number of different states and nucleotide-bound ring configurations (Baker and Sauer, 2012). Moreover, based on equilibrium and kinetic studies, two subunits in a CIpX hexamer do not appear to bind ATP, two bind ATP weakly, and two bind ATP strongly (Hersch et al., 2005; Stinson et al., 2013). ATP binding to subunits with weak affinity drives conformational changes required for the CIpX ring to hydrolyze ATP and perform mechanical work (Stinson et al., 2013). ATP hydrolysis and coupled mechanical work by CIpX rings cannot depend on a strictly sequential mechanism, as variants with numerous ATPase-inactive subunits still unfold and degrade protein substrates in solution (Martin et al., 2005) and in the single-molecule RWERWE studies here. Moreover, a strictly sequential mechanism should generate a clear sequence of translocation step sizes, which we do not observe. Finally, a model should account for the fact that ATP hydrolysis is substantially slower during CIpXP unfolding of native substrates than during translocation (Kenniston et al., 2003).

The models depicted in Fig. 7A and 7B meet the criteria described above and provide a quantitative framework for understanding CIpXP unfolding and translocation. CIpX rings are designated as active (X) or inactive (iX) with the number of bound ATPs specified by a trailing number. Thus, X4 is an active ring with four ATPs, and iX2 is an inactive ring with two ATPs. X3 and X4 rings are active. In agreement with biochemical studies (Stinson et

al., 2013), all other rings are inactive and must bind additional ATP and/or change conformation to become an active X4 or X3 ring. When a natively folded protein domain cannot enter the axial channel of an X4 or X3 ring, ATP hydrolysis and product release result either in a futile power stroke or in a power stroke that causes unfolding (Fig. 7A). For simulations with the kinetic constants shown, the rates of these processes, conformational changes, and ATP-binding steps result in single-exponential unfolding kinetics ($R^2 = 0.999$) and a τ_{unf} of 6 s, a value close to τ_{unf} for V13P titin. Decreasing just the rate constant for unfolding in the model produces longer pre-unfolding dwells, as we observe for the Halo, V15P titin, and WT titin domains. The model also predicts hydrolysis of an average of ~5 ATPs for each V13P domain that CIpXP unfolds and higher ATP consumption in proportion to the increased unfolding times for more stable domains, as observed experimentally (Kenniston et al., 2003).

Once unfolding is successful, additional cycles of ATP hydrolysis drive translocation of the polypeptide chain as diagrammed in Fig. 7B. Again, only X4 and X3 rings are active. From the X4 ring, physical steps of 1–4 nm are taken depending upon which ATP-bound subunit hydrolyzes ATP or fires first. For example, initial firing of low-affinity subunit **a** results in a 1 nm step, initial firing of low-affinity subunit **b** results in a 2 nm step, and so on (Fig. 7C). From the X3 ring, firing of the **b** subunit results in a 1 nm step, whereas firing of the **c** and **d** subunits result in steps of 2 and 3 nm, respectively. For steps of 2, 3, or 4 nm, we assume that 2, 3, or 4 ATPs are hydrolyzed and/or released in rapid succession, generating a burst of power strokes that are not experimentally resolved. Simulations using the rate constants in Fig. 7B produce step-dwell distributions (Fig. S2) and step-size distributions close to the experimental distributions (Fig. S5). Step memory, which depends on the rates at which the X3 ring takes additional steps or recycles to X4, was also recapitulated (Fig. S6), but to a smaller extent than observed. In simulated data, for example, 38% of all 1 nm steps were followed by a second 1 nm step, whereas this value was 41% in the experimental data. In the absence of memory, only 29% of the next steps would also be 1 nm. Sen et al. (2013) reported almost complete loss of 4 nm steps at ATP concentrations near K_M. At low ATP concentrations, our model predicts that the population of X3 rings would increase substantially compared to X4 rings, reducing the average step size and fraction of 4 nm steps. The ATPase rate in our model is effectively determined by the slow conformational rearrangements needed to generate active X4 and X3 rings (2.2 s^{-1} for translocation; 0.5 s^{-1} for unfolding), predicting ~4-fold faster ATP hydrolysis during translocation than unfolding, as is experimentally observed during CIpXP degradation of native and denatured titin substrates (Kenniston et al., 2003). Thus, our model accounts for a broad range of experimental results. We were unable to match the experimental results using models in which CIpX conformational changes precede rather than follow ATP binding or in which X4 rings are the only active species.

Stochastic AND coordinated ATP hydrolysis

In our model, initial ATP hydrolysis in the X4 or X3 rings is probabilistic, as first proposed based on studies of CIpX rings with mixtures of active and inactive subunits (Martin et al., 2005). Contrary to arguments by Smith et al. (2011), a probabilistic or stochastic model does not imply that subunits act independently. Indeed, Martin et al. (2005) found that ATP-

hydrolysis activity was not strictly proportional to the number of ATPase active subunits and provided strong evidence that directional communication between neighboring subunits regulates ATP hydrolysis and mechanical activity. In crystal structures of hexameric CIpX rings, the nucleotide-binding pockets in each subunit that can bind ATP (loadable subunits) vary slightly (Glynn et al., 2009; Stinson et al., 2013), providing a basis for differential nucleotide affinities and for different probabilities of which subunit fires first. It is also possible, however, that interactions with the protein substrate determine which subunit fires first (Martin et al., 2005). For example, GYVG loops in the axial pore of CIpX are known to contact the ssrA tag and translocating substrates and to influence ATP-hydrolysis rates. Thus, an ATP-bound subunit whose pore loop was in direct contact with a translocating polypeptide or the ssrA tag might have a higher probability of firing first (Martin et al., 2008b; 2008c), and the highly variable chemical and conformational heterogeneity of an unfolded polypeptide chain could determine the stochastic nature of initial firing.

Following stochastic firing of a specific subunit in the CIpX ring, whether and how many additional subunits fire rapidly will depend on subunit-subunit communication. Although the details of such communication remain to be deciphered, we suggest one possibility. For example, firing of a given subunit might cause ATP-bound counter-clockwise subunits to fire or release nucleotide, so that initial firing in the **a, b, c**, or **d** subunits in X4 would result in hydrolysis/release of 1, 2, 3, or 4 ATPs and translocation steps of 1, 2, 3, or 4 nm, and initial firing of the **b, c**, or **d** subunits in X3 would result in hydrolysis/release of 1, 2, or 3 ATPs and physical steps of 1, 2, or 3 nm (Fig. 7C). Thus, a physical translocation step that began with a stochastic ATP-hydrolysis event could be followed by coordinated hydrolysis/release events, which could be programmed sequentially or stochastically. The choice of counter-clockwise versus clockwise propagation in the model is arbitrary.

With minor modifications, this model can also explain how RWERWE CIpXP could take steps of ~3 nm or larger using only two hydrolytically active wild-type subunits in the CIpX ring. As shown in Fig. 7D, multiple configurations of an X4 ring are possible for RWERWE CIpX. When W subunits occupy the **a** and **d** positions (Fig. 7D, left), initial firing of the **a** subunit could generate a 1 nm step, whereas initial firing of the **d** subunit could yield a 4 nm step, with ATP release from inactive subunits generating some power strokes. By contrast, RWERWE X4 configurations with wild-type subunits at the **b** or **c** positions (Fig. 7D, center and right) could result in 2 or 3 nm steps. Is it energetically feasible for ATP release to generate a power stroke? The highest force at which we recorded RWERWE CIpXP activity was ~10 pN. To drive a ~1 nm movement against this force requires ~1.5 kcal/mol (~2.5 kT) of energy. At the 2 mM ATP concentrations used for our experiments, a conformational change in the ATP-binding pocket that weakened affinity to ~30 mM would allow ATP dissociation to generate a favorable free-energy change of ~1.6 kcal/mol ($\Delta G = -RT\ ln$ (30 mM/2 mM)), making it plausible that ATP release drives a power stroke. ATP-loadable and unloadable subunits in the CIpX ring interconvert during function (Stinson et al., 2013), and thus the affinity of a given subunit for ATP could become substantially weaker as a consequence of structural changes in neighboring subunits. Why are the dwell times between physical steps in RWERWE CIpXP translocation so much longer than in wild-type

CIpXP translocation? The simplest possibility is that the presence of catalytically inactive R or E subunits at ring positions poised to fire requires a slow ring-resetting reaction.

Alternative models

Although the models in Fig. 7 explain our single-molecule results and are consistent with a wide range of observations, related models may do so equally well. For example, we model the active CIpX ring with five loadable subunits and one unloadable subunit (Stinson et al., 2013), but other ratios of loadable to unloadable subunits could work equally well. Similarly, we assume that only four ATPs bind to the CIpX ring based on biochemical results (Hersch et al., 2005), but the results could also be fit if ATP bound to each loadable subunit. The modeled arrangement of high-affinity and low-affinity subunits in the CIpX ring is also speculative.

In a very different model proposed by Sen et al. (2013), the number of ATPs bound to the CIpX ring solely determines the size of the subsequent physical step, which always ends with a nucleotide-free CIpX ring. Thus, they suggest that a 4 nm, 3 nm, and 2 nm steps are taken if 4, 3, or 2 ATPs are initially bound to the CIpX ring, respectively. Their model excludes the possibility of 1 nm steps. In conflict with biochemical experiments (Stinson et al., 2013), the Sen model requires CIpX rings with ATP bound only to two high-affinity subunits to be active. It also fails to account for the motor memory we observe or to explain why a broad mixture of physical-step sizes is observed at saturating concentrations of ATP. Sen et al. (2013) propose that P_i release is the force-sensitive step coupled to each power stroke, rather than ATP hydrolysis, ADP release, or ATP binding. In our view, the chemical step responsible for power strokes remains in question, as the P_i-release model depends upon untested assumptions and fails to account for our finding that RWERWE CIpXP can take steps of ~3 nm or longer.

Conformational switching

Conformational switching between ATP loadable and unloadable subunits in the CIpX ring, with concomitant changes in the identities of the subunits that bind ATP with high and low affinity, appears to be required for robust mechanical activity (Stinson et al., 2013). How can this requirement be rationalized in terms of the models shown in Fig. 7? One possibility is that conformational switching is directly involved in force generation for every power stroke. Another possibility is that the products of ATP hydrolysis are not properly ejected after some unfolding attempts or translocation steps. Loadable-unloadable conformational switching might eject these products and redefine the ATP affinities of individual subunits to reset the CIpX ring and allow resumption of translocation or unfolding attempts (Stinson et al., 2013). Pausing during CIpXP translocation may arise in this manner, with the greater pausing propensity of RWERWE CIpXP resulting from the presence of catalytically inactive subunits, which increase the probability that a translocation step finishes with a ring conformation that must be reset before activity resumes.

Importance of large and small step sizes

What role do large physical translocation steps play in CIpXP degradation? As a single 4 nm step takes ~35% as much time as four 1 nm steps, bigger physical steps may simply allow

faster translocation and thus faster degradation. We note, however, that translocation may represent a small fraction of the time required for degradation of many proteins. Another possibility is that a kinetic burst of power strokes is better able to unfold certain proteins, for example those with larger distances to the unfolding transition state. If large translocation steps are beneficial, then why has CIpXP evolved to take small steps as well? Small steps may allow CIpX to maintain a tighter grip on the substrate because more subunits are ATP bound (Nager et al., 2011), allowing more efficient transfer of force and increasing the probability of unfolding certain proteins.

Lessons for solution degradation

For multiple substrates, CIpXP degradation is substantially slower than predicted based on single-molecule rates of unfolding and translocation (Fig. 6A), indicating that commitment is the slowest step in solution degradation. Indeed, experiments suggest that native titin substrates are bound and released many times before being unfolded by CIpXP (Kenniston et al., 2005). Two factors can affect commitment times for CIpXP. First, the SspB adaptor, which binds both to the ssrA tag and to CIpX, increases V_{max} for protein degradation (Levchenko et al., 2000; Wah et al., 2002). If commitment is the slow step in degradation at substrate saturation, then SspB must make this step faster. Consistently, SspB reduces the time required for binding and unfolding in single-turnover experiments. For example, in single-turnover experiments at 30 °C, the time required for CIpXP binding and unfolding of GFP-ssrA is ~34 s in our experiment but ~17 s with SspB present (Martin et al., 2008a). Thus, SspB is likely to increase the probability of unfolding by increasing the average number of CIpXP unfolding attempts that occur before substrate dissociation and the need for rebinding. Second, the length of polypeptide bound in the axial pore of CIpXP influences commitment. For example, this length is ~15 residues for ssrA-tagged titin, Halo, and GFP substrates but 35–40 residues for the non-tagged domains of multi-domain substrates, including those in single-molecule experiments (Lee et al., 2001; Kenniston et al., 2005; Martin et al., 2008a). In single-turnover experiments performed in the presence of SspB at 30 °C, CIpXP degraded GFP followed by an unstructured C-terminal titin-ssrA domain almost twice as fast as GFP-ssrA and at rates similar to those observed for single-molecule unfolding (Martin et al., 2008a; Maillard et al., 2011; Sen et al., 2013). From a mechanistic perspective, a longer region of polypeptide in the axial pore of CIpXP should allow a tighter grip by the enzyme and thus reduce the probability of dissociation following a failed unfolding attempt. If longer unstructured degrons can speed degradation and result in a lower net cost in terms of ATP hydrolysis, then why are relatively short degrons used so often in biological systems? One possibility is that protein degradation typically occurs in energy-rich cellular environments and that longer degrons would open the possibility for truncation of the degron by non-specific proteases, preventing targeted degradation of the proper substrates by CIpXP and other AAA+ proteases.

Experimental Procedures

Proteins were expressed and purified as described in the Supplement. For single-molecule experiments, biotinylated CIpXP was attached to a laser-trapped bead, substrate containing a Halo domain covalently linked to biotinylated DNA was attached to another bead, and

enzyme-substrate tethers were formed. Measurements were performed under constant force at 18–22 °C using 2 mM ATP with ATP-regeneration and oxygen-scavenging systems as described (Aubin-Tam et al., 2011). Data were collected at 3 kHz sampling frequency and decimated for further analysis. Custom MATLAB scripts were used to calculate inter-bead distances, measure unfolding distances, measure pre-unfolding dwells from the end of one translocation event to the next unfolding event, determine average translocation velocity, and detect pauses. Individual translocation steps were identified using the chi-squared method (Kerssemakers et al., 2006), which requires input of the expected number of steps, estimated by taking the pair-wise distribution of decimated data subjected to a step-smoothing algorithm based on L1-regularization with independent noise (Little et al., 2011). We set a minimum detectable step-size threshold of 0.75 nm and combined smaller steps, including backward steps or slips, with previous and following steps by adding the dwell-weighted average (S_{avg}) of a small step (S) to the previous step (S-1) and subtracting S_{avg} from the following step (S+1). The dwell-weighted average is defined as:

$$S_{avg} = S \bullet (d_{S+1})/(d_S + d_{S+1})$$

where d_S is the dwell preceding a small step and d_{S+1} is the dwell following a small step. Kinetic simulations of the models shown in Fig. 7 are described in the Supplement.

Supplementary Material

Refer to Web version on PubMed Central for supplementary material.

Acknowledgments

This work was supported by grants from the NSF (Career Award 0643745, MCB-1330792), the NIH (GM-101988), the Singapore-MIT Alliance for Research and Technology (SMART) program, and HHMI. J.C.C. was supported by a GAANN fellowship from the U.S. Department of Education under Grant No. P200A090323. Y.S. was supported by a Samsung Scholarship from the Samsung Foundation of Culture. B.M.S. was supported by a Poitras pre-doctoral fellowship. T.A.B. is an employee of HHMI. We thank Jacob Kerssemakers for the MATLAB implementation of his step-finding algorithm.

References

Aubin-Tam M-E, Olivares AO, Sauer RT, Baker TA, Lang MJ. Single-molecule protein unfolding and translocation by an ATP-fueled proteolytic machine. Cell. 2011; 745:257–267. [PubMed: 21496645]

Baker TA, Sauer RT. CIpXP, an ATP-powered unfolding and protein-degradation machine. Biochim. Biophys. Acta. 2012; 1823:15–28. [PubMed: 21736903]

Barkow SR, Levchenko I, Baker TA, Sauer RT. Polypeptide translocation by the AAA+ CIpXP protease machine. Chem. Biol. 2009; 16:605–612. [PubMed: 19549599]

Carrion-Vazquez M, Oberhauser AF, Fowler SB, Marszalek PE, Broedel SE, Clarke J, Fernandez JM. Mechanical and chemical unfolding of a single protein: a comparison. Proc. Natl. Acad. Sci. USA. 1999; 96:3694–3699. [PubMed: 10097099]

Glynn SE, Martin A, Nager AR, Baker TA, Sauer RT. Structures of asymmetric CIpX hexamers reveal nucleotide-dependent motions in a AAA+ protein-unfolding machine. Cell. 2009; 739:744–756. [PubMed: 19914167]

Joshi SA, Hersch GL, Baker TA, Sauer RT. Communication between CIpX and CIpP during substrate processing and degradation. Nat. Struct. Mol. Biol. 2004; 77:404–411. [PubMed: 15064753]

Kenniston JA, Baker TA, Fernandez JM, Sauer RT. Linkage between ATP consumption and mechanical unfolding during the protein processing reactions of an AAA+ degradation machine. Cell. 2003; 774:511–520. [PubMed: 12941278]

Kenniston JA, Burton RE, Siddiqui SM, Baker TA, Sauer RT. Effects of local protein stability and the geometric position of the substrate degradation tag on the efficiency of CIpXP denaturation and degradation. J. Struct. Biol. 2004; 746:130–140. [PubMed: 15037244]

Kenniston JA, Baker TA, Sauer RT. Partitioning between unfolding and release of native domains during CIpXP degradation determines substrate selectivity and partial processing. Proc. Natl. Acad. Sci. USA. 2005; 702:1390–1395. [PubMed: 15671177]

Kerssemakers JW, Munteanu EL, Laan L, Noetzel TL, Janson ME, Dogterom M. Assembly dynamics of microtubules at molecular resolution. Nature. 2006; 442:709–712. [PubMed: 16799566]

Kim YI, Burton RE, Burton BM, Sauer RT, Baker TA. Dynamics of substrate denaturation and translocation by the CIpXP degradation machine. Mol. Cell. 2000; 5:639–648. [PubMed: 10882100]

Lee C, Schwartz MP, Prakash S, Iwakura M, Matouschek A. ATP-dependent proteases degrade their substrates by processively unraveling them from the degradation signal. Mol. Cell. 2001; 7:627–637. [PubMed: 11463387]

Levchenko I, Seidel M, Sauer RT, Baker TA. A specificity-enhancing factor for the CIpXP degradation machine. Science. 2000; 28:2354–2356. [PubMed: 11009422]

Li H, Carrion-Vazquez M, Fernandez JM. Point mutations alter the mechanical stability of immunoglobulin modules. Nat. Struct. Biol. 2000; 7:1117–1120. [PubMed: 11101892]

Little MA, Steel BC, Bai F, Sowa Y, Bilyard T, Mueller DM, Berry RM, Jones NS. Steps and bumps: Precision extraction of discrete states of molecular machines. Biophys J. 2011; 101:477–485. [PubMed: 21767501]

Maillard RA, Chistol G, Sen M, Righini M, Tan J, Kaiser CM, Hodges C, Martin A, Bustamante C. ClpX(P) Generates Mechanical Force to Unfold and Translocate Its Protein Substrates. Cell. 2011; 145:459–469. [PubMed: 21529717]

Martin A, Baker TA, Sauer RT. Rebuilt AAA + motors reveal operating principles for ATP-fuelled machines. Nature. 2005; 437:1115–1120. [PubMed: 16237435]

Martin A, Baker TA, Sauer RT. Protein unfolding by a AAA+ protease is dependent on ATP-hydrolysis rates and substrate energy landscapes. Nat. Struct. Mol. Biol. 2008a; 15:139–145. [PubMed: 18223658]

Martin A, Baker TA, Sauer RT. Pore loops of the AAA+ CIpX machine grip substrates to drive translocation and unfolding. Nat. Struct. Mol. Biol. 2008b; 15:1147–1151. [PubMed: 18931677]

Martin A, Baker TA, Sauer RT. Diverse pore loops of the AAA+ CIpX machine mediate unassisted and adaptor-dependent recognition of ssrA-tagged substrates. Mol. Cell. 2008c; 29:441–550. [PubMed: 18313382]

Nager AR, Baker TA, Sauer RT. Stepwise unfolding of a β-barrel protein by the AAA+ CIpXP protease. J. Mol. Biol. 2011; 413:4–16. [PubMed: 21821046]

Popa I, Berkovich R, Alegre-Cebollada J, Badilla CL, Rivas-Pardo JA, Taniguchi Y, Kawakami M, Fernandez JM. Nanomechanics of Halo tag tethers. J. Am. Chem. Soc. 2013; 735:12762–12771. [PubMed: 23909704]

Sauer RT, Baker TA. AAA+ proteases: ATP-fueled machines of protein destruction. Annu. Rev. Biochem. 2011; 80:587–612. [PubMed: 21469952]

Sen M, Maillard RA, Nyquist K, Rodriguez-Aliaga P, Pressé S, Martin A, Bustamante C. The CIpXP protease unfolds substrates using a constant rate of pulling but different gears. Cell. 2013; 155:636–646. [PubMed: 24243020]

Shin Y, Davis JH, Brau RR, Martin A, Kenniston JA, Baker TA, Sauer RT, Lang MJ. Single-molecule denaturation and degradation of proteins by the AAA+ CIpXP protease. Proc. Natl. Acad. Sci. USA. 2009; 10:19340–19345. [PubMed: 19892734]

Smith DM, Fraga H, Reis C, Kafri G, Goldberg AL. ATP binds to proteasomal ATPases in pairs with distinct functional effects, implying an ordered reaction cycle. Cell. 2011; 144:526–538. [PubMed: 21335235]

Stinson BM, Nager AR, Glynn SE, Schmitz KR, Baker TA, Sauer RT. Nucleotide binding and conformational switching in the hexameric ring of a AAA+ machine. Cell. 2013; 753:628–639. [PubMed: 23622246]

Thompson MW, Maurizi MR. Activity and specificity of *Escherichia coli* CIpAP protease in cleaving model peptide substrates. J. Biol. Chem. 1994; 269:18201–18208. [PubMed: 8027081]

Wah DA, Levchenko I, Baker TA, Sauer RT. Characterization of a specificity factor for an AAA+ ATPase: assembly of SspB dimers with ssrA-tagged proteins and the CIpX hexamer. Cherm. Biol. 2002; 9:1237–1245.

Research Highlights

- CIpXP takes physical translocation steps of 1–4 nm in a stochastic pattern
- The stability of degron-proximal structure determines substrate unfolding rates
- One ATP-hydrolysis event can drive more than one power stroke
- Commitment to unfolding is the slow step in solution degradation

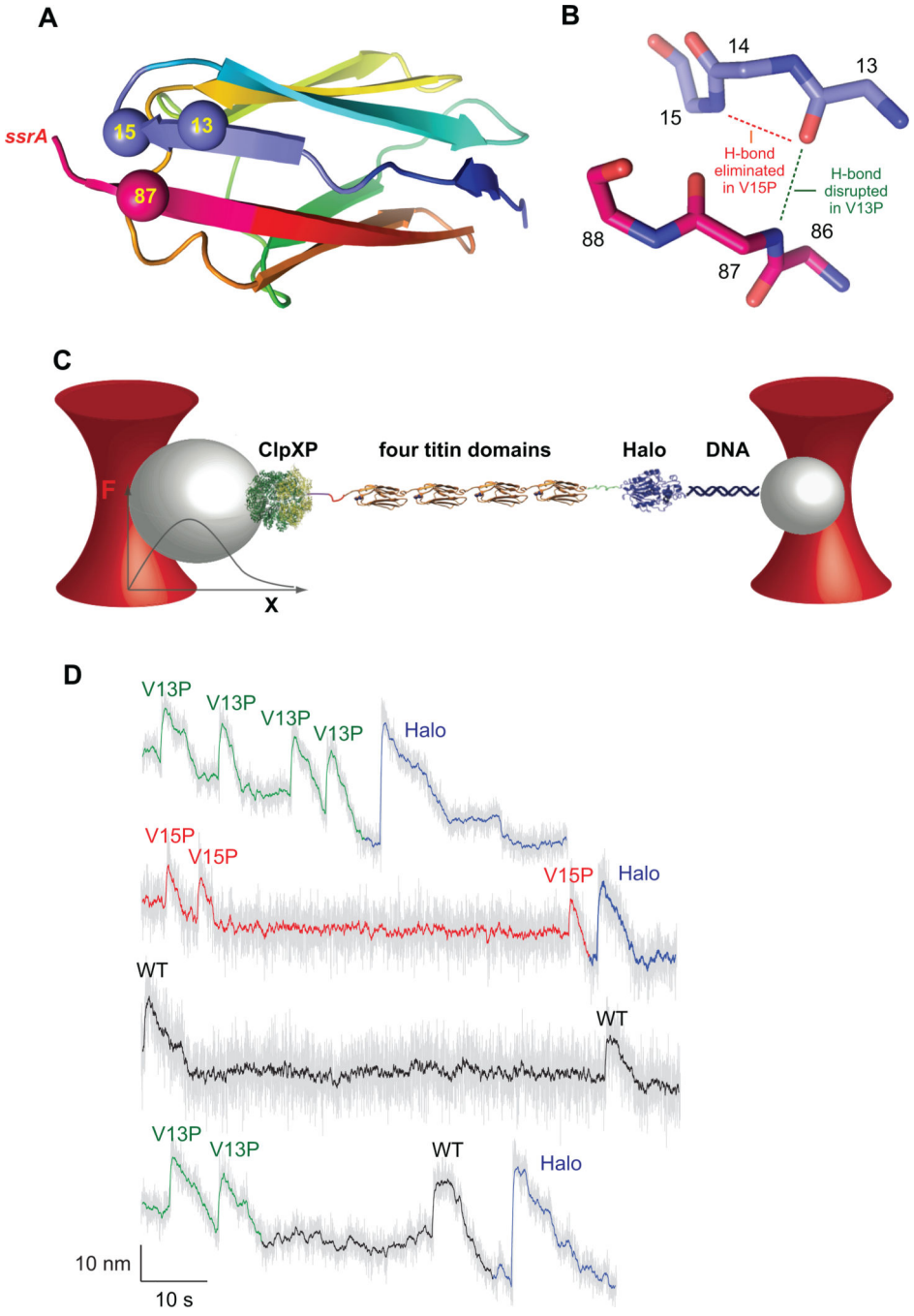

Fig. 1.

Single-molecule unfolding and translocation of substrates. (**A**) Cartoon structure of titin[127] (pdb code, 1tit), colored from the N terminus (blue) to the C terminus (red). Spheres show α carbons for residues 13, 15, and 87. ClpXP pulling on a C-terminal ssrA tag is resisted by local structure, including β-sheet hydrogen bonding between the C-terminal β strand and the β strand with residues 13 and 15. (**B**) The V13P and V15P mutations disrupt hydrogen bonds that directly or indirectly stabilize the titin[127] domain. (**C**) Experimental setup for single-molecule assays of ClpXP unfolding and translocation. ClpXP is attached to one laser-

trapped bead and has engaged the ssrA tag of a multi-domain substrate consisting of four titin domains and a Halo domain, which is attached to a second laser-trapped bead via a DNA linker. (**D**) Trajectories for CIpXP unfolding and translocation of multi-domain substrates. Unfolding of individual domains increases bead-bead distance (upward movement), whereas translocation decreases bead-bead distance (downward movement). After completed translocation of one domain, there is a variable dwell time before CIpXP unfolds the next domain. The dwell baselines before and after titin unfolding events are spaced as expected for the end-to-end distance of a native titin domain (4.4 nm) or native titin plus the linker to the Halo domain.

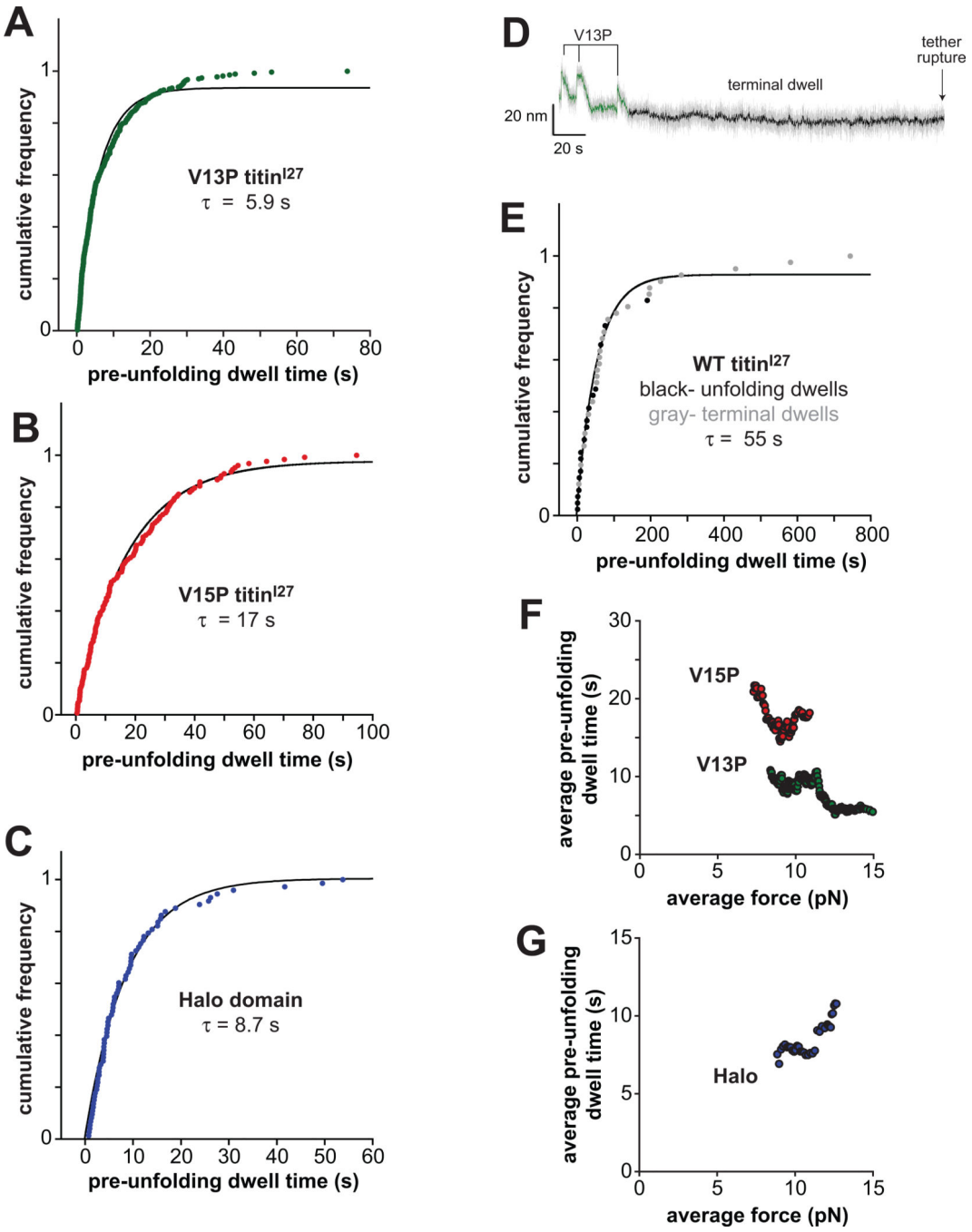

Fig. 2.

CIpXP unfolding of domains in multi-domain substrates. (**A–C**) Distributions of pre-unfolding dwell times for the V13P, V15P, and Halo domains. In each plot, the solid line is a non-linear-least-squares fit to $y=A*(1-\exp(-t/\tau_{unf}))$. (**D**) For the Halo-WT-V13P-V13P-V13P-ssrA substrate, long "terminal" dwells were often observed following unfolding and translocation of the V13P titin domains. (**E**) CIpXP unfolding of wild-type titin^{127} domains. Black symbols are pre-unfolding dwells; gray symbols are "terminal" dwells. The line is a fit to $y=A*(1-\exp(-t/\tau_{unf}))$. (**F**) Plots of average force versus average pre-unfolding dwell

times (calculated over a moving 50-point window) for the V13P and V15P domains. (**G**) Plot of average force versus average pre-unfolding dwell times (calculated over a moving 40-point window) for the Halo domain. See also Figs. S1, S4, and S7.

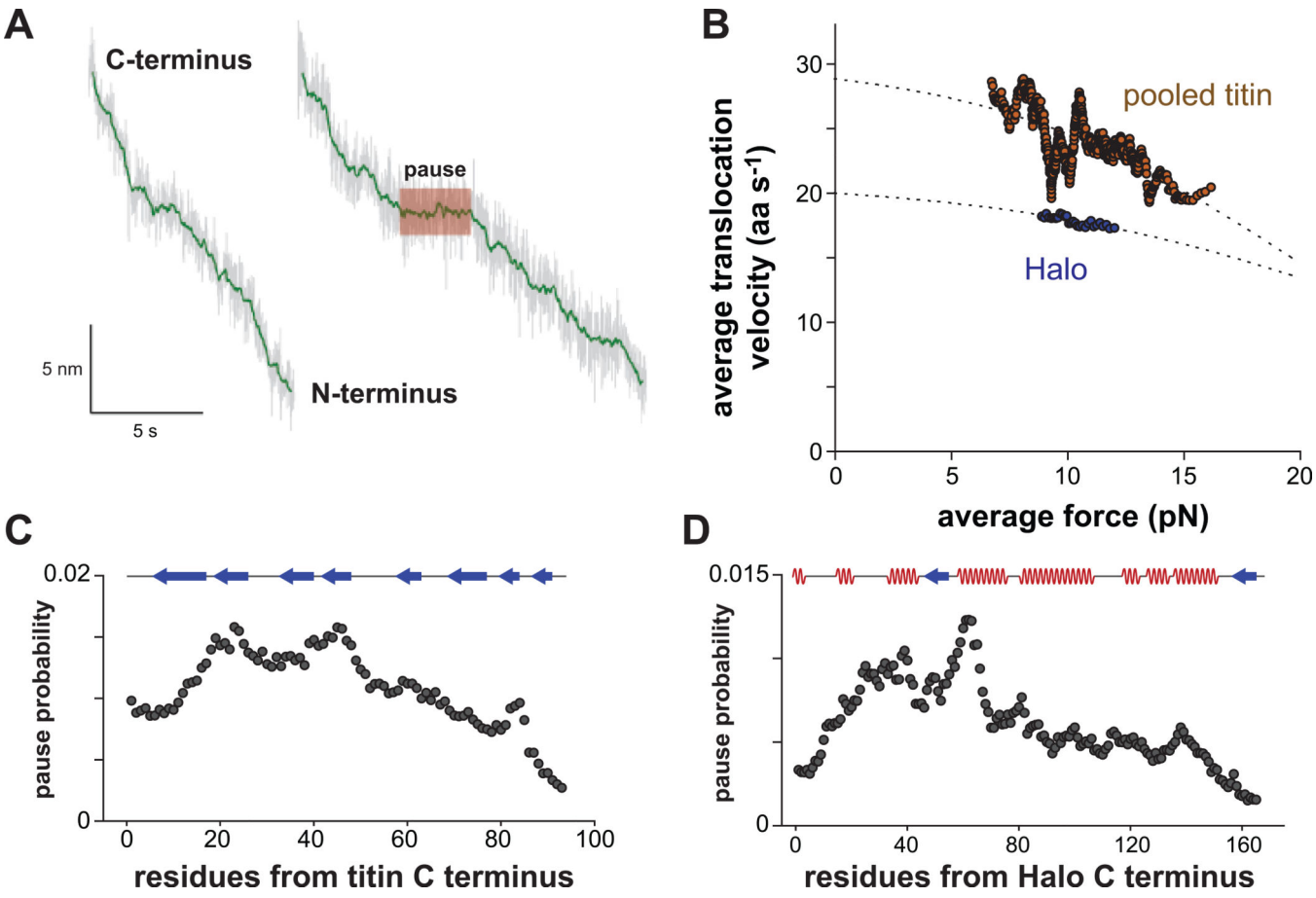

Fig. 3.

Translocation and pausing. (**A**) V13P translocation traces proceeding with approximately constant velocity (left panel) or with a pause (right panel). (**B**) Plots of average force versus average translocation velocity were calculated over a moving 50-point window for the V13P and V15P domains and over a 40-point window for the Halo domain. The lines are fits to a single-barrier Boltzmann equation $v = v_0 \bullet (1.05)/(1+0.05 \bullet \exp(F \bullet 0.7/kT))$ where F is the average force and kT is 4.1 pN•nm at room temperature. (**C**) Probability of pausing of CIpXP along the length of a titin domain (N = 25). (**D**) Probability of pausing of CIpXP along the length of a Halo domain (N = 24). Secondary structure in the native structure is indicated schematically in panels C and D (arrows represent β strands; zigzag lines represent α helices).

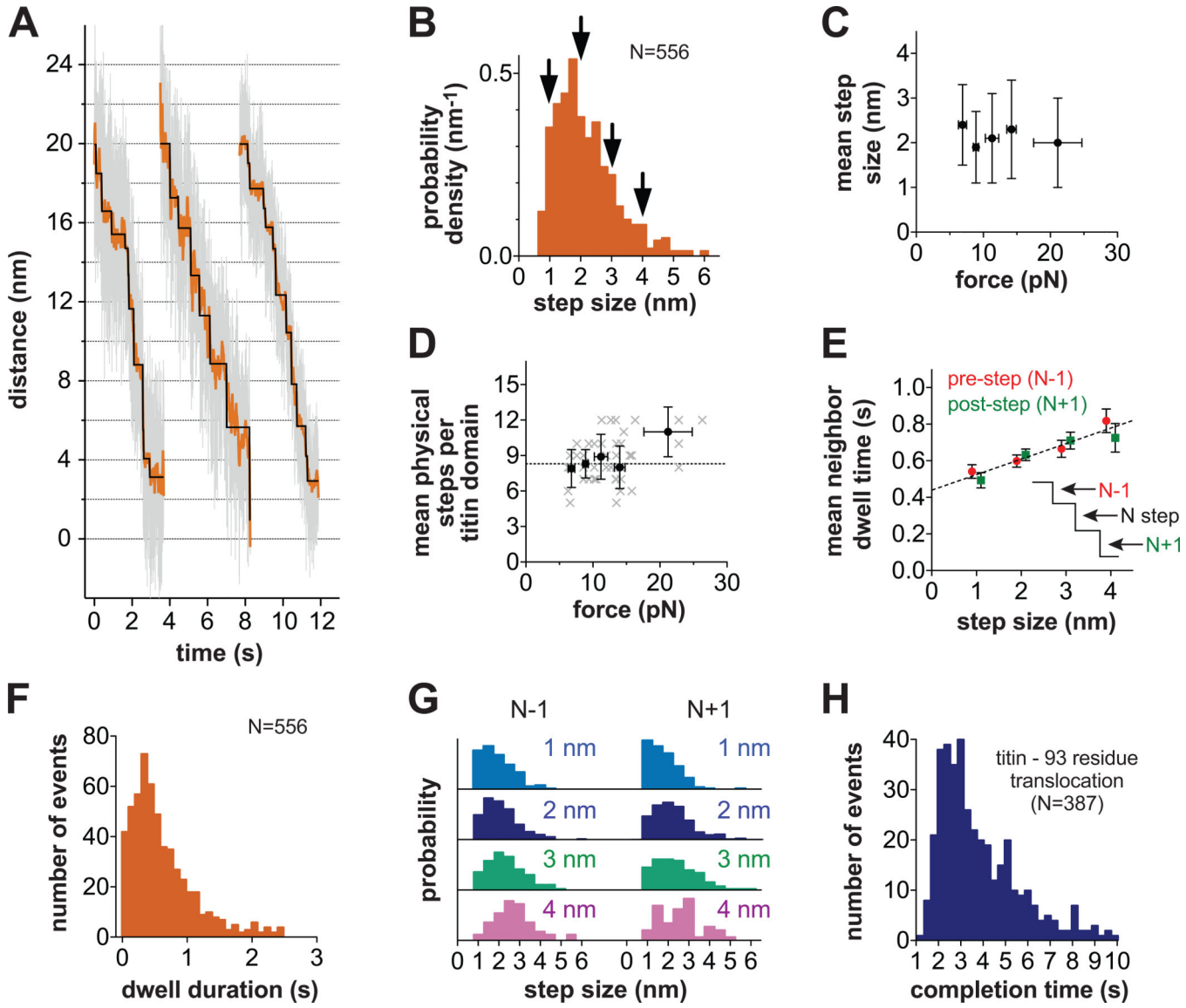

Fig. 4.

Physical steps during titin translocation. (**A**) Representative stepping in CIpXP translocation trajectories. Raw data were decimated to 500 Hz (gray) or 50 Hz (orange). Chi-square fits to the 50 Hz data are shown in black. (**B**) Distribution of physical steps sizes during titin translocation. (**C**) Mean physical step size during titin translocation as a function of force. X- and Y-error bars are ± 1 SD (N = 70–221). (**D**) Mean number of physical steps required to translocate an 89-residue titin domain and 4-residue linker as a function of force (black squares). X- and Y-error bars are ± 1 SD (N = 6– 20). Gray X's are step numbers from individual translocation trajectories. (**E**) Mean dwell times ± SEM (N = 45–236) before (red) or after (green) physical steps of 1–4 nm (pre- and post-step values are offset slightly on the x-axis for clarity). (**F**) Distribution of dwell times preceding steps of all sizes during titin translocation. (**G**) Occurrence of steps of different size either before (N−1) or after (N +1) physical steps of 1–4 nm. (**H**) Distribution of times required to complete translocation of

89-residue titin domains and subsequent 4-residue linkers after subtracting pauses. See also, Figs. S2, S3, S5, S6, and S8.

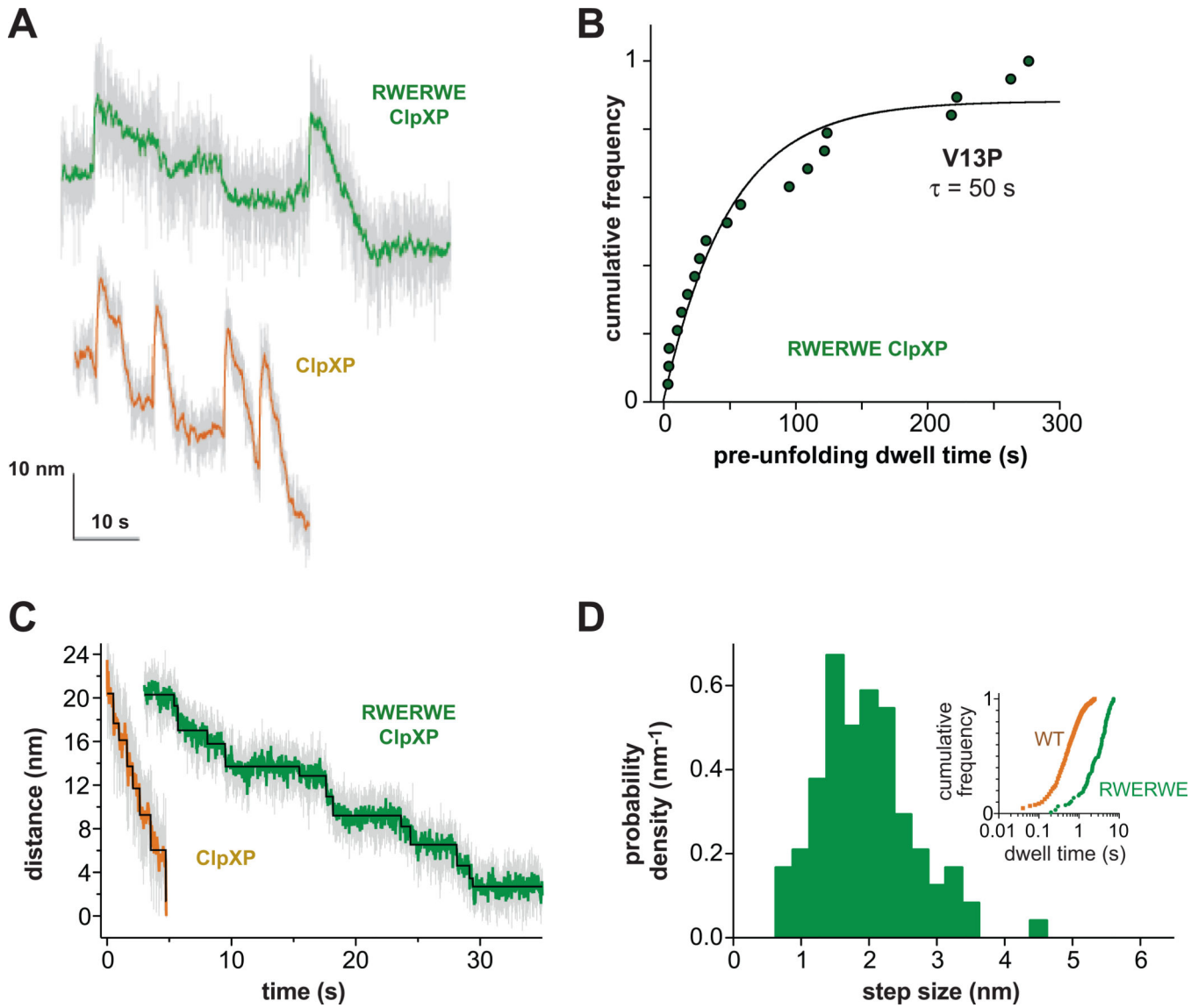

Fig. 5.

Unfolding and translocation by RWERWE CIpXP. (**A**) V13P unfolding and translocation traces for RWERWE CIpXP (top) and CIpXP with six active subunits (bottom). (**B**) Distributions of RWERWE CIpXP pre-unfolding dwell times for the V13P domain. The line is a non-linear-least-squares fit to $y = A*(1-\exp(-t/\tau_{unf}))$. (**C**) Representative stepping in titin V13P translocation by CIpXP (orange) and RWERWE CIpXP (green). Decimation and fits (black) are described in Fig. 4A. (**D**) Distribution of RWERWE physical step sizes. Inset- Cumulative frequency distributions of dwell times preceding steps for CIpXP (orange) or RWERWE CIpXP (green). See also Fig. S8.

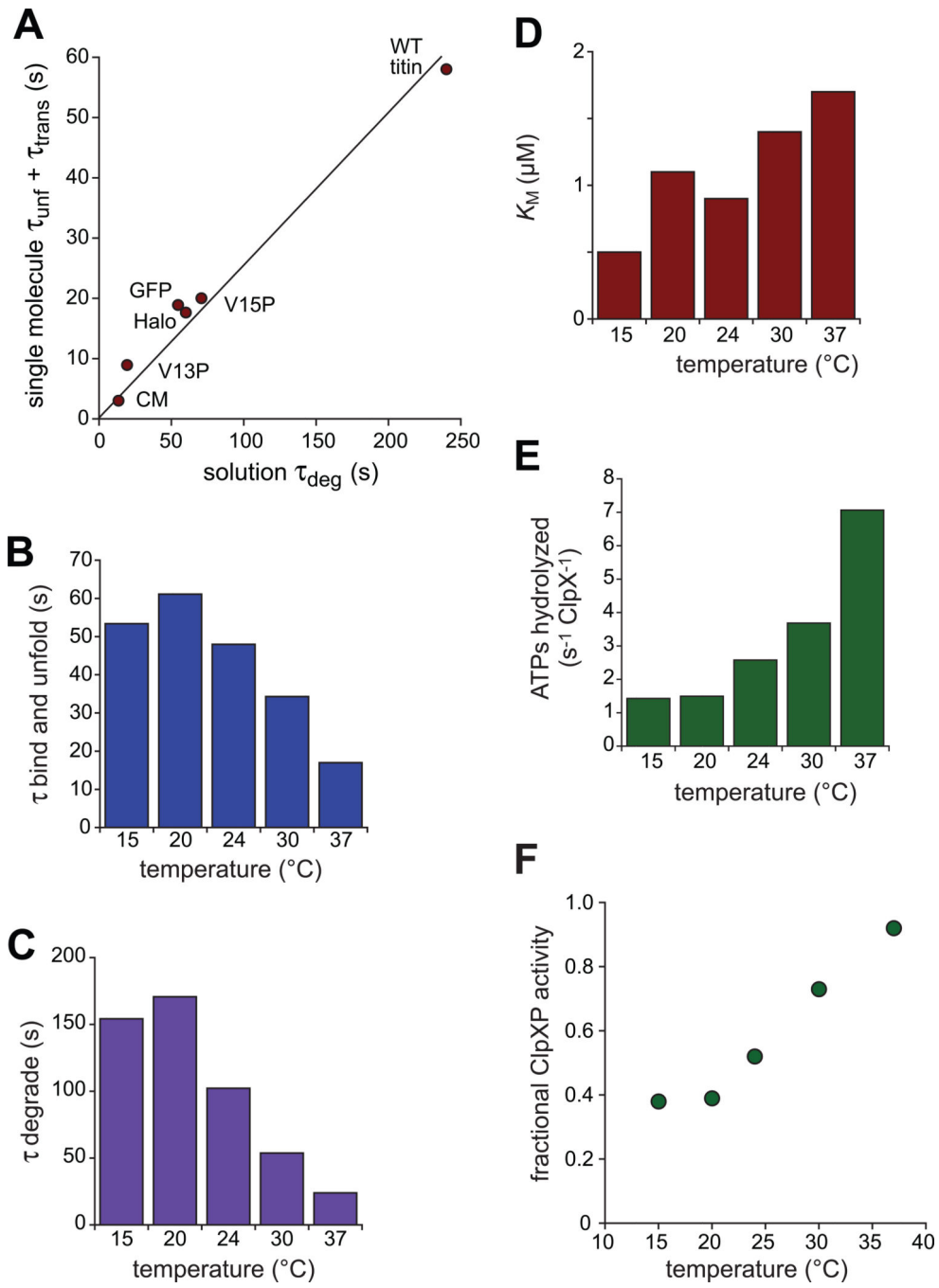

Fig. 6.

Solution degradation times are poorly predicted by single-molecule unfolding and translocation times. (**A**) Plot of average times required for solution degradation (τ_{deg}) of titin-ssrA (WT), V15P-titin-ssrA (V15P), V13P-titin-ssrA (V13P), carboxymethylated titin-ssrA (CM), GFP-ssrA (GFP), and Halo-ssrA (Halo) versus $\tau_{unf} + \tau_{trans}$ times from single-molecule experiments (Kim et al., 2000; Kenniston et al., 2003; Sen et al., 2013; this work). Times for titin and GFP degradation were determined at 30 °C, whereas single-molecule experiments and Halo-ssrA degradation were performed at room temperature. Degradation

is slower at lower temperatures (see panel C), which would increase the discrepancy between the solution and single-molecule results. τ_{unf} values were determined under load and could be different at zero force, but V13P and V15P τ_{unf} values (Fig. 2E) would not increase 4-fold and the Halo τ_{unf} value appears to decrease (Fig. 2F). (**B**) τ values for single-turnover binding and unfolding of GFP-ssrA (0.5 μM) by CIpXP (10 μM $CIpX^{\Delta N}$; 20 μM CIpP) at different temperatures. (**C**) τ_{deg} values ($1/V_{max}$) at different temperatures determined from Michaelis-Menten plots of steady-state rates of degradation of different concentrations of GFP-ssrA by $CIpX^{\Delta N}$ (0.3 μM) and CIpP (0.9 μM). (**D**) K_M values for GFP-ssrA degradation at different temperature (conditions as in panel C). (**E**) Rates of CIpXP ATP hydrolysis at different temperatures by $CIpX^{\Delta N}$ (0.3 μM) in the presence of CIpP (0.9 μM) and GFP-ssrA (20 μM). (**F**) Fractional activity of CIpXP at different temperatures calculated as $(\tau_c + \tau_{unf} + 5\ s)/\tau_{deg}$, where the $\tau_c + \tau_{unf}$ value is taken from panel B and 5 s is the estimated time for translocation of GFP-ssrA.

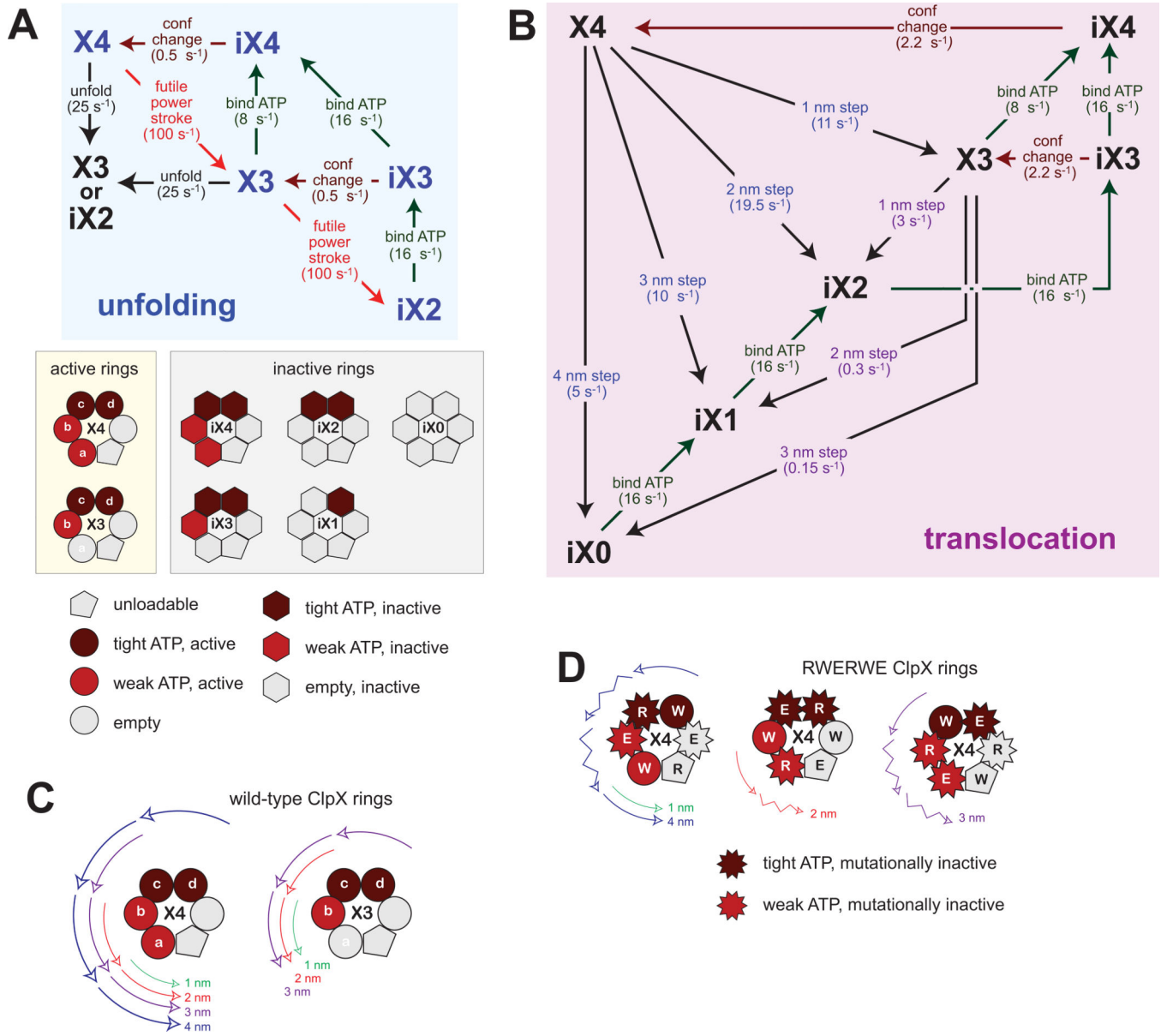

Fig. 7.

Mechanochemical models for CIpXP function. X4 and X3 rings are hydrolytically and mechanically active. iX3, iX2, iX1, and iX0 rings are inactive. Numbers after the X are bound ATPs. In the cartoons of the CIpX hexamer, dark red subunits bind ATP tightly, red subunits bind ATP weakly, and light gray subunits do not bind ATP. (**A**) Unfolding model. ATP hydrolysis in the X4 or X3 rings results in an unfolding power stroke, which allows translocation to begin, or in a futile power stroke. ATP-binding reactions are represented by green arrows and conformational changes by dark red arrows. For simplicity, ATP binding to iX0 or iX1 rings is not shown in this panel, ATP-dissociation reactions are not included, and different configurations of nucleotide-bound subunits in the X3 ring are not considered. Pseudo first-order rate constants for ATP-association reactions are for saturating concentrations of ATP. The mechanical stability of a native protein determines the rate of

the unfolding reaction; other rates are determined by the properties of CIpXP. The rate constants in parenthesis give exponential unfolding kinetics (τ_{unf} ~6 s). (**B**) Translocation model. Depending on which ATP-bound subunit in the X4 or X3 rings hydrolyzes ATP first, physical translocation steps of 1, 2, 3, or 4 nm are taken (black arrows). A physical step of N nm is associated with N hydrolysis/release events. Numbers in parentheses are rate constants that were adjusted to provide a reasonable fit to experimental data. (**C**) In the cartoons shown, initial ATP hydrolysis in subunits of X4 or X3 rings (labeled **d, c, b**, or **a**) result in very fast ATP hydrolysis/release events that generate power strokes (arrows) in the ATP-bound counter-clockwise subunits, generating physical translocation steps of 4, 3, 2, or 1 nm, respectively. (**D**) As shown on the left, if wild-type (W) subunits occupy the **d** and **a** positions in X4 rings of RWERWE CIpX, then translocation steps of 1 nm (subunit **a** fires first) or 4 nm (subunit **d** fires first) are taken. When subunit **d** fires first, ATP is released from the counter-clockwise inactive **c** (R) and **b** (E) subunits to generate power strokes (crooked arrows). If wild-type (W) subunits occupy the **b** or **c** positions in the X4 ring (center and right, respectively), then initial hydrolysis in these subunits results in steps of 2 or 3 nm, respectively, again with ATP release from counter-clockwise inactive subunits generating power strokes (crooked arrows). See also Figs. S2, S5, and S6.